

Article

Study of Intumescent Coatings Growth for Fire Retardant Systems in Naval Applications: Experimental Test and Mathematical Model

Elpida Piperopoulos ^{1,*}, Gabriele Grifò ², Giuseppe Scionti ¹, Mario Atria ³, Luigi Calabrese ¹, Giancarlo Consolo ² and Edoardo Proverbio ¹

¹ Department of Engineering, University of Messina, Contrada di Dio-Sant'Agata, 98166 Messina, Italy

² Department of Mathematical and Computer Sciences, Physical and Earth Sciences, Vill.S.Agata, 98166 Messina, Italy

³ Colorificio Atria, Contrada Camarro Formeca, 91028 Partanna (TP), Italy

* Correspondence: epiperopoulos@unime.it

Abstract: Onboard ships, fire is one of the most dangerous events that can occur. For both military and commercial ships, fire risks are the most worrying; for this reason they have an important impact on the design of the vessel. The intumescent coatings react when heated or in contact with a living flame, and a multi-layered insulating structure grows up, protecting the underlying structure. In this concern, the aim of the paper is to evaluate the intumescent capacity of different composite coatings coupling synergistically modeling and experimental tests. In particular, the experiments have been carried out on a new paint formulation, developed by Colorificio Atria S.r.l., in which the active components are ammonium polyphosphate or pentaerythritol. The specimens were exposed to a gas-torch flame for about 70 s. The degree of thermal insulation of the coating was monitored by means of a thermocouple placed on the back of the sample. In order to get insights into the intumescent mechanism, experimental data was compared with the results of a mathematical model and a good agreement is detected. Furthermore, a predictive model on the swelling rate is addressed. The results highlight that all coatings exhibit a clear intumescent and barrier capacity. The best results were observed for coating enhanced with NH_4PO_3 where a regular and thick, porous char was formed during exposure to direct flame.

Keywords: naval fires; intumescent coating; mathematical model



Citation: Piperopoulos, E.; Grifò, G.; Scionti, G.; Atria, M.; Calabrese, L.; Consolo, G.; Proverbio, E. Study of Intumescent Coatings Growth for Fire Retardant Systems in Naval Applications: Experimental Test and Mathematical Model. *Coatings* **2022**, *12*, 1180. <https://doi.org/10.3390/coatings12081180>

Academic Editor: Natalia V. Kamanina

Received: 12 July 2022

Accepted: 11 August 2022

Published: 15 August 2022

Publisher's Note: MDPI stays neutral with regard to jurisdictional claims in published maps and institutional affiliations.



Copyright: © 2022 by the authors. Licensee MDPI, Basel, Switzerland. This article is an open access article distributed under the terms and conditions of the Creative Commons Attribution (CC BY) license (<https://creativecommons.org/licenses/by/4.0/>).

1. Introduction

Fires onboard ships, unfortunately, are causes of human and environmental disasters. Fires can cause damage to the boat structure. The consequence of this, in the worst cases, can be the sinking of the ship, with loss of human life and/or spillage of pollutants into the sea, which damage the marine environment and the coast. The last naval fire that occurred in the Mediterranean Sea was on 18 February 2022 aboard a Grimaldi passenger ferry that traveled off the northern coast of the Greek island of Corfu, carrying 237 passengers and 51 crew members [1]. But there are several accidents involving boats that caught fire while they were at sea and turned out to be fatal. This is the case, for example, of the Norman Atlantic [2]. On the night of the 27th December 2014, the ferry was traveling from Igoumenitsa (Greece) to Ancona when it caught fire. The rescues were very complicated, over a long time: some lifeboats were destroyed by flames, and there was a storm and the sea was very rough. Eleven deaths and about twenty missing were confirmed.

The ship and marine structures are composed of vertical and horizontal areas separated by structural elements with and without thermal insulation. Fire irreparably damages the ship structures, which lose their geometrical shape and consequently their stability, collapsing. Therefore, the use of appropriate materials can increase the ability of each

ship structure to resist the fire effects, which means improving the fire resistance limit, which will guarantee the time necessary for rescue operations [3]. A passive approach to control the fire reaction is to use coatings onboard ship capable of increasing both thermal insulation and fire stability [4]. Intumescent coatings are reactive coatings and are identified as an excellent solution for protecting structural steel load-bearing systems during fire [5]. In contact with heat, and even more so with fire, the intumescent coatings swell to form a foamed carbon with low density and low thermal conductivity; therefore, preventing the temperature increase in the steel which could cause structural instability and/or progressive failure [6,7]. So, these thin coatings swell on heating to form a highly insulating char, protecting steel members and preventing them from reaching critical temperatures that could cause them to fail. Intumescent coatings are among the most efficient ways of fire retarding flammable materials. The coatings swell under the influence of heat and form a thick porous charred layer, which perfectly insulates the substrate against an excessive increase of temperature and oxygen access [8]. In fact, during the swelling, process oxygen is sequestered, decreasing the level of oxidizing from the surrounding environment. Moreover, swelling involves a succession of reactions, mostly endothermic, which absorb heat, decreasing the temperature of the coating [9]. The choice of components for an intumescent fire-retardant coating has an essential effect on the swelling rate and, accordingly, the charred mass formation, its thickness and its density.

Intumescent coatings are usually composed of a polymeric matrix with added organic and inorganic components [10,11]. Additives are normally an acid source (e.g., ammonium polyphosphate), which acts as a catalyst, a carbonific compound (generally pentaerythritol) and a foaming agent (normally melamine). The acid source breaks down to create a mineral acid that dehydrates the carbonific to produce the carbon char and, at the same time, the spumific decomposes in gaseous products, allowing the char swelling [12]. As a result of the activation of the process, a thick protective carbonaceous layer is formed. This insulating layer is the result of a perfect balance between chemical phenomena and transport phenomena. This interaction strongly depends on the components of the formulation. The right balance between the components guarantees an insulating and protective layer. Mathematical models could be useful tools for the optimization of highly performing intumescent materials, predicting their reaction to fire [13]. Cirpici et al. [14] developed a theoretical model for quantifying expansion of intumescent coating under different heating conditions. Anderson et al. [15] studied a mathematical model that described the physical processes of an intumescent system, by taking into account mass and energy control volumes. Experimental data from thermogravimetric and differential scanning calorimeter analysis were employed to validate the numeric study. Di Blasi et al. [16] investigated a mathematical model on a composite system consisting of a substrate and an intumescent coating subjected to a variable radiative heat flux (20–200 kW/m²). Often the mathematical model is developed on very simplified descriptions of the physical processes, which take part in the intumescence, based on a one-dimensional enthalpy equation coupled with different relations for the volume change [17]. Transport models of intumescent coatings have generally been applied to irradiation phenomena, but analyses and validations have been carried out showing a very limited correspondence [17–19].

To couple, synergistically, modeling and experimental tests could be a suitable approach to get insights to assess the intumescent coatings reaction that occurs when heated on, in contact with a living flame. In this concern, the aim of the paper is to evaluate the intumescent capacity of two different composite coatings, in which the active components are ammonium polyphosphate and pentaerythritol. In particular, the experimental test was performed exposing the samples to a direct gas-torch flame for about 70 s (identified as optimal time to assess the barrier and intumescence capacity of the coatings). The degree of thermal insulation and intumescence of the coating was monitored by means of a thermocouple placed on the back of the sample and digital camera, respectively. With the purpose of providing an improvement in knowledge about the intumescent mechanisms, experimental data are finally compared with a predictive mathematical model. The scope

of the research is, preliminarily, to develop a simplified model, describing, based on the comparison with experimental tests, both the thermal resistance, expansion and oxidation of the intumescent coatings.

2. Materials and Methods

2.1. Coating Production

The studied coating is a new formulation of Colorificio Atria S.r.l. (Colorificio ATRIA S.r.l. Partanna (TP), Italy). The starting material is an Atria's proprietary acrylic coating (named iC, intumescent Coating). In order to increase the intumescent property, the use of ammonium polyphosphate (Budenheim KG, Budenheim, Germany) was increased (APiC, Ammonium Polyphosphate intumescent Coating). In fact, the ammonium polyphosphate promotes the intumescent process acting as catalyst [20]. The acronym codes of all the studied products are shown in Table 1. The formulations were deposited (about 76 μm) on ASTM A1008 carbon steel supports (Q-LAB CORPORATION, Westlake, OH, USA), 140 mm \times 70 mm \times 0.8 mm to perform the fire resistance tests. The chemical composition of the supporting panel is 0.60% max Manganese, 0.15% max Carbon, 0.030% max Phosphorus, 0.035% max Sulfur. Furthermore, to better understand the intumescent insulating properties of the realized products, an uncoated carbon steel plate was used as reference (named uC, unCoated).

Table 1. Codes and specifications of the investigated samples.

Acronym Code	Specifications
iC	Intumescent coating
APiC	Intumescent coating enhanced with NH_4PO_3
uC	uncoated

2.2. Morphological Characterization

Morphological analysis was performed using environmental scanning electron microscopy (SEM, FEI Quanta 450, Thermo Fisher Scientific, Waltham, MA, USA) working in Low Vacuum, at 20.00 kV. A Large Field Detector (LFD) and a spot size of 3.5 were used. Additionally, chemical analysis was performed along with the morphological studies using energy-dispersive X-ray spectroscopy (EDAX, Ametek, Tokyo, Japan) at an acceleration voltage of 20 kV.

2.3. Flame Test

The fire-reaction behavior of the coatings was studied by conducting a specifically designed flame test (Figure 1). The specimens were exposed to a propane gas-torch flame (flame temperature 2253 K) at a distance of 1 cm from the specimen (300 kW/m^2) for about 70 s. The heat flow was calculated considering the propane calorific value ($14 \text{ kW/g}\cdot\text{h}$) and propane consumption, measuring the gas can weight before and after the test, over the investigated time. Five measurements were conducted for each coating. The reaction of the coating was recorded by two cameras, the first placed in front of the specimen, the second along its cross section to monitor the profile evolution. The temperature was monitored using an infrared camera (Optris GmbH, Berlin, Germany). In addition, a K-thermocouple placed behind the steel coated support (Figure 1b) was used to evaluate the thermal insulation degree provided by the coating. A further test, using a lower heat flow (150 kW/m^2), decreasing the intensity of the torch flame, was conducted on APiC sample to better identify the early stages of the intumescence process.

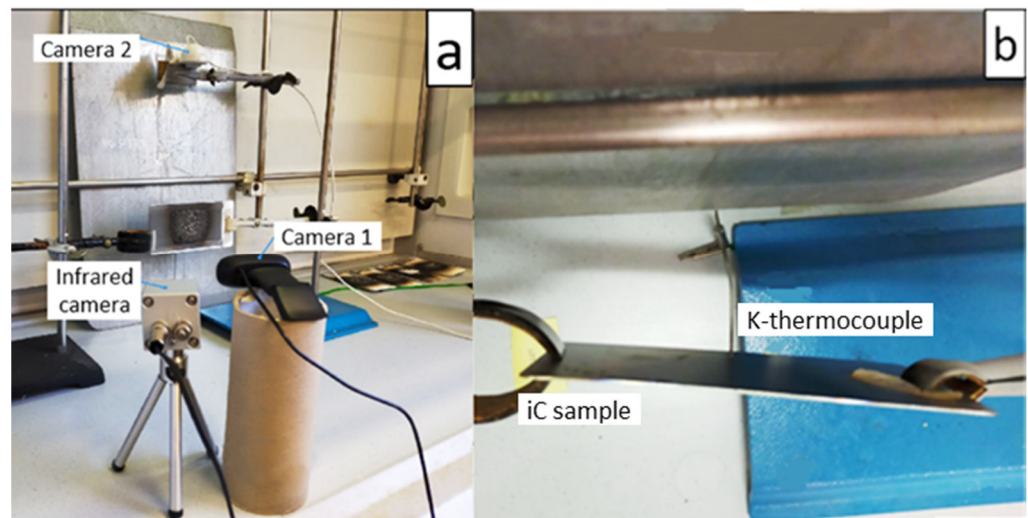


Figure 1. Flame test set-up. Cameras and infrared camera (a), K-thermocouple (b).

2.4. Mathematical Model

In order to gain more insights into the observed phenomenon, a mathematical modeling of intumescence process was addressed to predict the time evolution of back face temperature as well as of the thickness of growing and ablative layers for sample APiC. In particular, to better appreciate the growth processes at short time, the predictive mathematical model was performed by using, as reference, the curve with the lowest heat flow (150 kW/m^2). The use of the lowest heat flux has been selected to have a less abrupt kinetics process, to better discriminate the phenomena that occur during swelling. This was useful to allow an adequate comparison between the theoretical and experimental aspects. The model accounts for the decomposition of intumescent coatings, subject to the external fire source, the swelling process that originates when temperature reaches an activation threshold and heat transfer in the reactive coating and in the substrate. When the coating is exposed to a source of heat and the critical temperature is reached, the inorganic acid, present in the formulation, undergoes a thermal decomposition. The blowing agent is then activated, causing an endothermic reaction that absorbs heat from the substrate and decomposes to release a large amount of gaseous products, trapped in the coating, causing the formation of a low density and thick material, which acts as thermal barrier for the steel substrate [21]. Assuming a uniform distribution of heat source over the sample, a one-dimensional model is here considered. In particular, the geometry consists of a three-layer structure, defined as follows (see Figure 2):

1. A substrate, made by steel, whose thickness (x_{steel}) is kept fixed, so unaffected by the intumescent process;
2. An ablative layer, made by a filled acrylic matrix, whose thickness ($f(t) - x_{steel}$) reduces in time as the material ablation due to pyrolysis starts;
3. A growing layer, mostly made by char, whose thickness ($g(t) - f(t)$) increases in time due to the swelling process, following the decomposition of the ablative layer.

Time t_1 represents the time at which the reaction in the ablative layer starts.

In order to model the phenomena occurring during the early stages of the intumescent process, in line with some literature [13], herein, the solidified char layer is not explicitly taken into account. In particular, the early stage evolution of the system can be described as follows:

- At time $t = 0$, the system is composed by two layers, the substrate and the intumescent coating, and the homogeneous heat source is applied on the top face of the sample;
- At time t_1 , the top face achieves a critical temperature T_S that gives rise to the swelling process and to decomposition of the ablative layer.

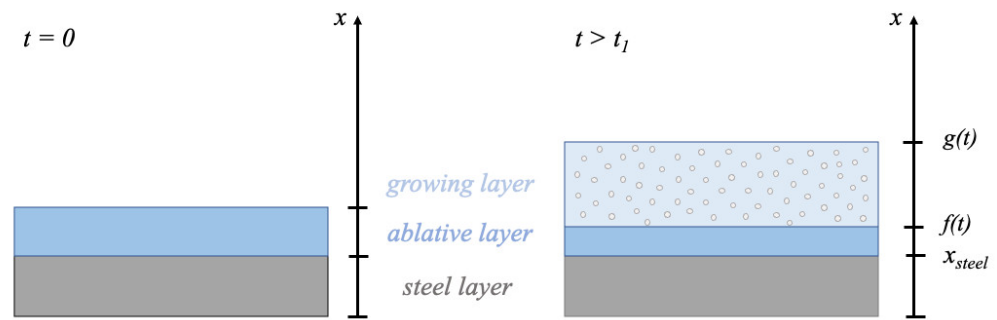


Figure 2. Schematics of the system under the assumption of a homogeneous thermal source.

In line with existing literature [13,17], the above phenomena can be described by means of a set of free-boundary nonlinear partial differential equations, consisting of nonsteady heat (Fourier) equations for each layer. The model reads:

$$\begin{cases} \rho_{steel} C_{steel} \frac{\partial T(x,t)}{\partial t} - \lambda_{steel} \Delta T(x,t) = 0 & \forall x \in [0, x_{steel}] \\ \rho_{abla} C_{abla} \frac{\partial T(x,t)}{\partial t} - \lambda_{abla} \Delta T(x,t) = -L_V \mathfrak{M}(T(x,t)) & \forall x \in [x_{steel}, f(t)] \\ \rho_{grow} C_{grow} \frac{\partial T(x,t)}{\partial t} - \lambda_{grow} \Delta T(x,t) = 0 & \forall x \in [f(t), g(t)] \end{cases} \quad (1)$$

where ρ represents the material density, C the specific heat, λ the thermal conductivity and the subscripts “steel”, “abla” and “grow” stand for “steel substrate”, “ablative layer” and “growing layer”, respectively.

Spatio-temporal evolution of temperature is given by $T(x,t)$ and $\Delta T = \frac{\partial^2 T}{\partial x^2}$. The heat transfer in the ablative layer accounts for an empirical Arrhenius-type law, with a prefactor L_V , that can be expressed as:

$$\mathfrak{M}(T(x,t)) = \begin{cases} 0 & \text{for } T(x,t) < T_s \\ -\rho_{abla} k_f \exp\left(\frac{-E}{R T(x,t)}\right) & \text{for } T(x,t) \geq T_s \end{cases} \quad \forall (x,t) \in [x_{steel}, f(t)] \times \mathbb{R}^+ \quad (2)$$

where k_f is a pre-exponential factor, E is the activation energy and R is the universal gas constant.

This law allows for correlation of the temperature with the velocity of the reducing boundary as follows:

$$\frac{\partial f(t)}{\partial t} = - \int_{x_{steel}}^{f(t)} \frac{\mathfrak{M}(T(x,t))}{\rho_{abla}} dx \quad (3)$$

Differently, the expansion of the top boundary is related to the gradient of gases pressure [22,23] and its speed is given by:

$$\frac{\partial g(t)}{\partial t} = - \frac{\chi \rho_{gas} R}{\mu M \theta} \frac{\partial T(x,t)}{\partial x} \quad (4)$$

where χ represents the material permeability, μ the fluid viscosity, M is the gas molecular mass and θ the layer’s porosity.

Finally, the system (1)–(2) is closed with the following boundary and initial conditions:

$$\begin{aligned} -\lambda_{grow} \frac{\partial T(x,t)}{\partial x} &= h(T(x,t) - T_{ex}) + \varepsilon \sigma (T(x,t) - T_{ex}^4) - \alpha \Phi(t) & x = g(t) \\ -\lambda_{grow} \frac{\partial T(0,t)}{\partial x} &= h(T(0,t) - T_{ex}) + \varepsilon \sigma (T(0,t) - T_{ex}^4) & \forall t \in \mathbb{R}^+ \\ T(x,0) &= T_{ex} & \forall x \in [0, x_{steel} + x_{abla}] \\ f(0) &= g(0) = x_{steel} + x_{abla} \end{aligned} \quad (5)$$

where h denotes the convective heat exchange coefficient, ε the emissivity of the front face ($x = g(t)$), σ the Stefan-Boltzmann constant, α the absorptivity of the front face, T_{ex} is the initial room temperature and $\Phi(t)$ the time dependent heat flux. Note that, both steel-ablative and ablative-growing interfaces are assumed to be in perfect contact and the

continuity of gradients and temperature is guaranteed. Herein, debonding phenomena generally occurring between the layers when the material is exposed to prolonged fire have been here disregarded.

3. Results and Discussion

3.1. Morphological Characterization

The morphology of the analyzed samples, at low magnification, appears similar (Figure 3). In particular, the APiC sample has a denser texture. All coatings show a regular structure, mainly composed of cubic and spherical particles of pentaerythritol, melamine and ammonium polyphosphate. The size of these particles is less than 25 μm . The analyzed area is homogeneous, without cracks, and the particles are well bonded by the acrylic matrix.

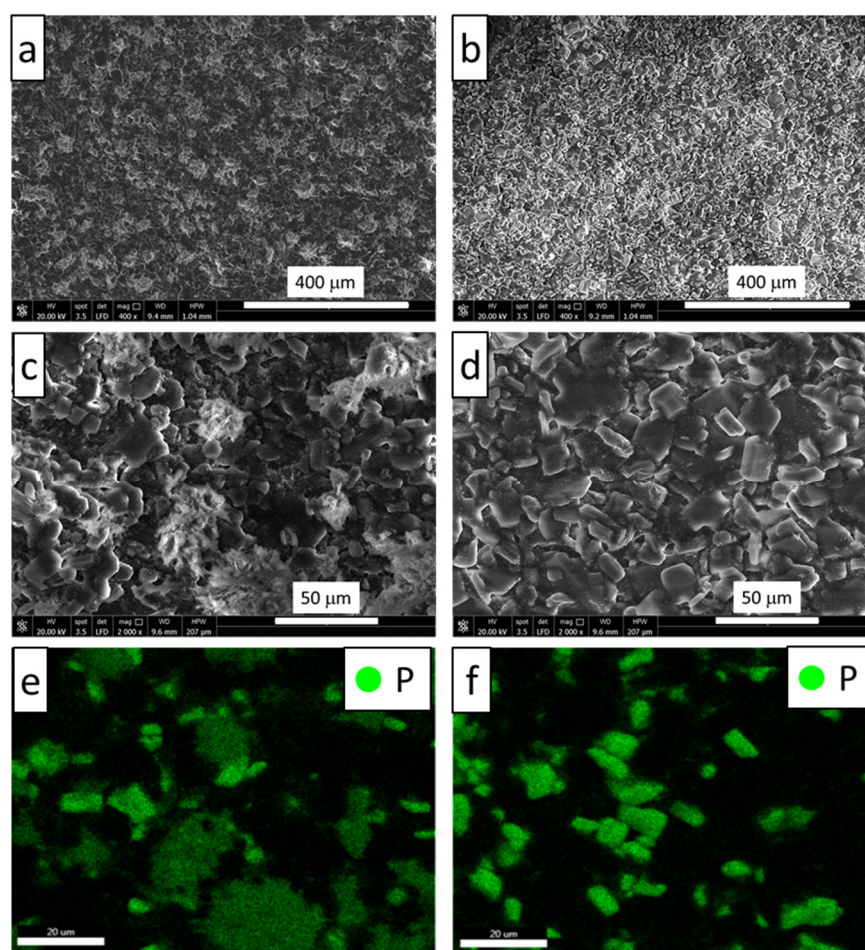


Figure 3. SEM images of the investigated formulations, (a,c) iC; (b,d) APiC, and respective EDX mappings, (e,f).

At higher magnifications, an inhomogeneous structure can be noted, as confirmed by the EDX mapping analysis, in particular for iC sample, where some particles agglomerations are present. The EDX analysis detects a greater amount of well distributed phosphorous in APiC sample, due to the presence of a higher percentage of ammonium polyphosphate (compare Figure 4a,b). The images reported in Figure 4 refer to the SEM images in Figure 3a,b respectively. The peaks mainly refer to C and O, amenable to the organic matrix, but to added melamine and pentaerythritol, also. Peaks of Mg, Na, Al, Ti, Ca and Si are furthermore evident, due to the presence of metals oxides and silica, in particular for iC sample (Figure 4c). TiO_2 , as it is well known, can improve the thermal performance and char morphology of the intumescent coating [24]. In Figure 4d, the EDX mapping of APiC

sample is reported. In this case, C, O and P are the more visible elements, as confirmed by the EDX spectrum in Figure 4b. The higher amount of P (compare Figure 3e,f) and, consequently, the larger scale of the y -axis in Figure 4b makes peaks of the other filler components less evident.

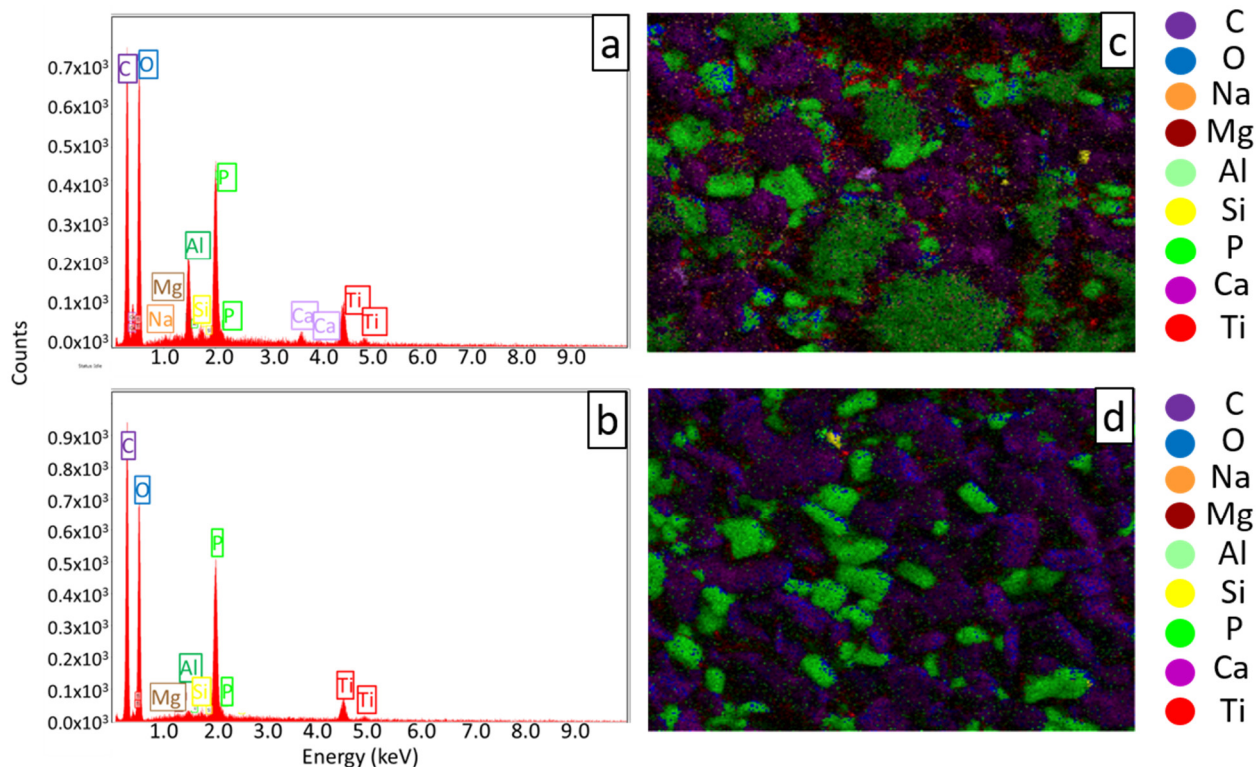


Figure 4. EDX spectra and mapping for iC (a,c) and APiC (b,d).

3.2. Flame Test Results

In Figure 5, the images of each specimen at time $t = 0$ and after 65 s ($t = 65$ s) of flame exposure are reported. In addition, the images detected by the infrared camera and the section of the specimen during the test are shown. The uncoated steel plate (uC) is considered as reference.

The intumescent character of the coatings is clearly shown. After 65 s of flame exposure, for the uncoated steel, the surface temperature, detected by the infrared camera, is higher than 700 K for a wide area of the sample, evidently higher than the coated samples. Analyzing the section images of the investigated formulations, a thicker intumescence product is observed for the samples APiC.

By analyzing the temperatures detected by the K-thermocouple (placed on the back side of the sample, as visually evidenced in Figure 1b), both the coatings present an insulation property. Compared to the uncoated plate, a temperature decrease of almost 200 K is obtained. In particular, the sample APiC at 65 s, records a temperature of 455.4 K, considerably lower than the uC and the iC specimen (650.9 and 479.4 K, respectively). Furthermore, by turning off the flame, the samples tend to quickly decrease the temperature, reaching temperatures below 373 K, in about 80 s as reported in Figure 6.

As already highlighted, the significant insulating action of the intumescent coating is noted. In particular, the graph in Figure 6 confirms the good insulation behavior of APiC sample. Furthermore, a lower heating rate is observable for the coated sample, particularly for the APiC specimen. As can be easily understood, as the flame was removed, the samples cooling took place. For the uncoated sample, the cooling is more sudden (about 4.53 K/s), whereas the coated samples cool down more slowly (about 1.62 K/s), showing a cooling rate almost similar for the different coatings. The values reached after 80 s are 358 and 354 K, respectively, for iC and APiC. In addition, the APiC curve related to the lowest heat flow of

150 kW/m² is reported. In this case, the temperature reached by the K-thermocouple at 65 s of flame exposition is about 375 K, approximately 80 K lower than the one subjected to the highest heat flow. Consequently, after the flame interruption, the K-temperature reaches about 320 K in 80 s.

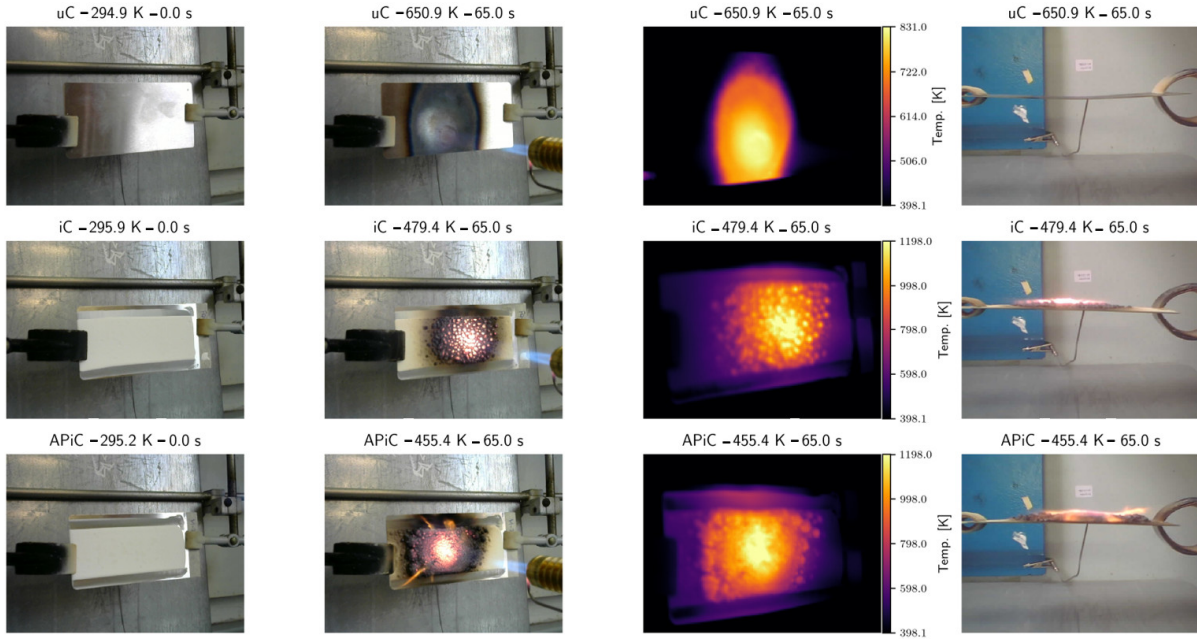


Figure 5. Images obtained by the used cameras of the investigated specimens, digital camera at 0 s and at 65 s (**first and second column**), infrared camera at 65 s (**third column**) and digital camera in cross section at 65 s (**last column**).

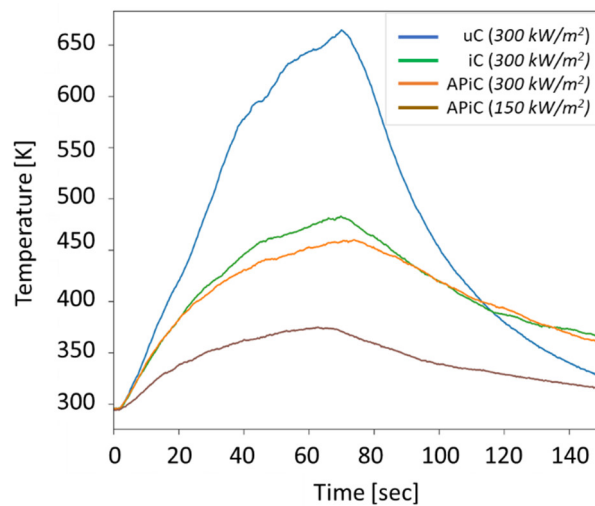


Figure 6. Temperature recorded by the K-thermocouple, up to the end of the test for each investigated sample, uC (blue line), iC (green line), APiC at a heat flow of 300 kW/m² (orange line) and APiC at 150 kW/m² (brown line). Note that, at $t = 70$ s, the flame is turned off.

Figure 7 shows section profiles of the coatings during intumescence, while in Table 2, the respective temperatures recorded by the thermocouple placed on the back of the specimen and the thickness of the sample are indicated for 25, 40, 65 and 80 s of flame test.

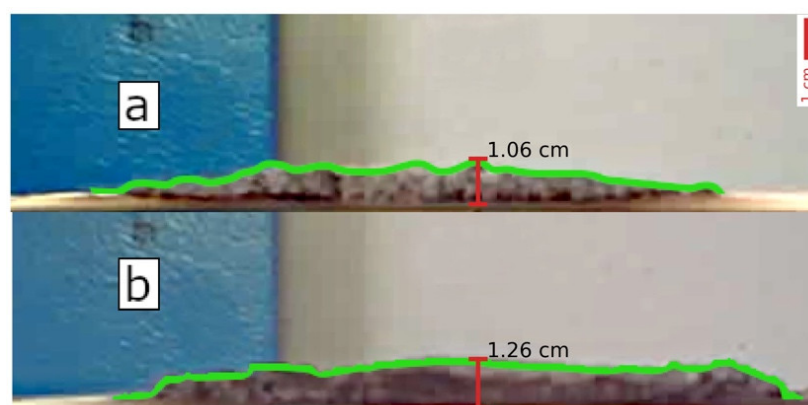


Figure 7. Sections of the intumescences during the fire test for the respective investigated samples, (a) iC, (b) APiC at 300 kW/m².

Table 2. Temperatures recorded by K-thermocouple and intumescence thicknesses as a function of time.

Sample	25 s	40 s	65 s	80 s
iC (300 kW/m ²)	410.4 ± 32.2 K 6.4 ± 0.13 mm	450.65 ± 25.3 K 8.1 ± 0.21 mm	480.4 ± 20.4 K 9.8 ± 0.22 mm	458.9 ± 28.5 K 10.6 ± 0.20 mm
APiC (300 kW/m ²)	401.9 ± 21.3 K 6.1 ± 0.17 mm	432.4 ± 30.4 K 10.0 ± 0.22 mm	457.4 ± 34.2 K 12.2 ± 0.21 mm	449.1 ± 20.3 K 12.7 ± 0.20 mm
APiC (150 kW/m ²)	344.1 ± 29.6 K 3.1 ± 0.20 mm	363.3 ± 33.2 K 6.6 ± 0.14 mm	374.2 ± 33.3 K 10.5 ± 0.21 mm	358.2 ± 35.1 K 10.5 ± 0.22 mm

Both iC and APiC coatings shows a clear intumescent behavior with the formation of a porous foamed char during the fire exposure. However, as evidenced in Figure 7, the section of the intumescent product of APiC appears more regular and thicker than iC one (green line in Figure 7). Furthermore, the porous char appears well-distributed in a larger area of the coated specimen. Moreover, comparing the results reported in Table 2, at 25 s of flame exposure, even if the thickness of iC specimen is higher, the insulation property of APiC is slightly evident (the average recorded maximum temperature is 410.4 and 401.9 K, respectively). This result is due to the fact that thickness is not the only characteristic that influences the insulating property of the material, but a fundamental role is played by the density of the intumescent [13]. Generally, the lower the density, the greater the insulating power [25]. The density of the produced material, obviously, depends on the swelling process and, therefore, on the constituent components of the formulation [26]. This behavior is noticed also at 40 s of flame exposure, when iC specimen shows a back temperature of 450.65 K and APiC sample, about 18 K lower (432.4 K). In this case, the thickness of APiC sample is higher than iC, as observed at longer times (80 s), when the flame is out and specimens are cooling down. The temperatures are, respectively, 458.9 and 449.1 K. The final thickness for the APiC specimen is 12.7 mm, and for the iC specimen is 10.6 mm. This behavior should be due to the higher amount of ammonium polyphosphate in the coating formulation. In fact, the component acts as a catalyst, giving the way to the sequence of actions that lead to swelling and consequently to the production of the intumescence [20]. Additionally, the values of the characteristics of the APiC sample, at the lowest heat flow are reported in the table. As evidenced, the temperatures reached by the K thermocouple is lower than the ones showed by the APiC at 300 kW/m², as well as the thickness, which does not exceed 10.5 mm. Even if the heat flow is lower than the one used for the other coated samples, the thickness observed at 80 s, when the test is concluded, is similar to the iC one. This is due to the highest ammonium polyphosphate added in the APiC samples, that promotes the intumescent process. As observed, the results presented a

dispersion in the recorded temperature data. An analytical approach taken to the results could be effective to enhance the obtained results [27–29].

3.3. Mathematical Model Results

In this section, we aim at describing the time evolution of the key parameters involved into the early stages of the intumescence process. To achieve this goal, we compare the experimental results obtained for the APiC sample, i.e., the material that exhibited the best thermal insulation response, subject to the flame with the lowest value of heat flux (150 kW/m^2) with the numerical ones predicted by the theoretical framework described in Section 2.4.

In particular, we will track the evolution of temperature on the back face $T(0,t)$, as well as the thicknesses of ablative $f(t)$ and growing $g(t)$ layers. To this aim, systems (1)–(5) are integrated numerically by means of the “Heat Transfer” module of COMSOL Multiphysics (v.6.0, COMSOL AB, Stockholm, Sweden) based on a finite-elements scheme. We used an adaptive and extremely fine mesh for both ablative and growing layers, whereas a fine mesh for the steel one. The real initial thicknesses values for all the layers have been employed, as specified in Table 3.

Table 3. Model parameters.

Symbol	Value	Unit	Description
x_{steel}	0.82	mm	Thickness of the steel layer
x_{abla}	0.76	mm	Initial thickness of the ablative layer
ρ_{steel}	7900	kg m^{-3}	Steel density
ρ_{abla}	1101.82	kg m^{-3}	Ablative material density
ρ_{gas}	1.5	kg m^{-3}	Gas density
C_{steel}	475	$\text{J kg}^{-1} \text{K}^{-1}$	Steel specific heat
C_{abla}	1884	$\text{J kg}^{-1} \text{K}^{-1}$	Ablative specific heat
C_{gas}	1005	$\text{J kg}^{-1} \text{K}^{-1}$	Gas specific heat
λ_{steel}	44.5	$\text{W m}^{-1} \text{K}^{-1}$	Steel thermal conductivity
λ_{abla}	0.198	$\text{W m}^{-1} \text{K}^{-1}$	Ablative material thermal conductivity
λ_{gas}	0.024	$\text{W m}^{-1} \text{K}^{-1}$	Gas thermal conductivity
T_{ex}	293.15	K	Room temperature
T_S	383	K	Activation temperature
k_f	10^7	s^{-1}	Pre-exponential factor
E	1.5×10^5	J mol^{-1}	Activation energy
R	8.32	$\text{J mol}^{-1} \text{K}^{-1}$	Universal gas constant
χ	2.2×10^{-15}	m^2	Material permeability
α	0.1	-	Front face absorptivity
ε	1	-	Front face emissivity
θ	0.9	-	Porosity of the growing layer
μ	4.5×10^{-5}	Pa s	Material viscosity
σ	5.67×10^{-8}	$\text{W m}^{-2} \text{K}^{-4}$	Stefan–Boltzmann constant
Φ	150	kW m^{-2}	Heating flux
h	20	-	Convective heat exchange coefficient
L_V	5×10^5	J kg^{-1}	Vaporization enthalpy
M	44	g mol^{-1}	Gas molecular mass

The numerical values of all the parameters appearing in the model are reported in Table 3. They are extracted from [17] in the literature, and from experimental estimations carried out on the specific painting under investigation.

The first, and most relevant, parameter to be taken into account is the temperature of the back face ($x = 0$), being the clearest indicator on the insulating character of the intumescent coating.

The comparison between experimental (symbol) and theoretical (solid line) is reported in Figure 8, revealing a satisfying agreement.

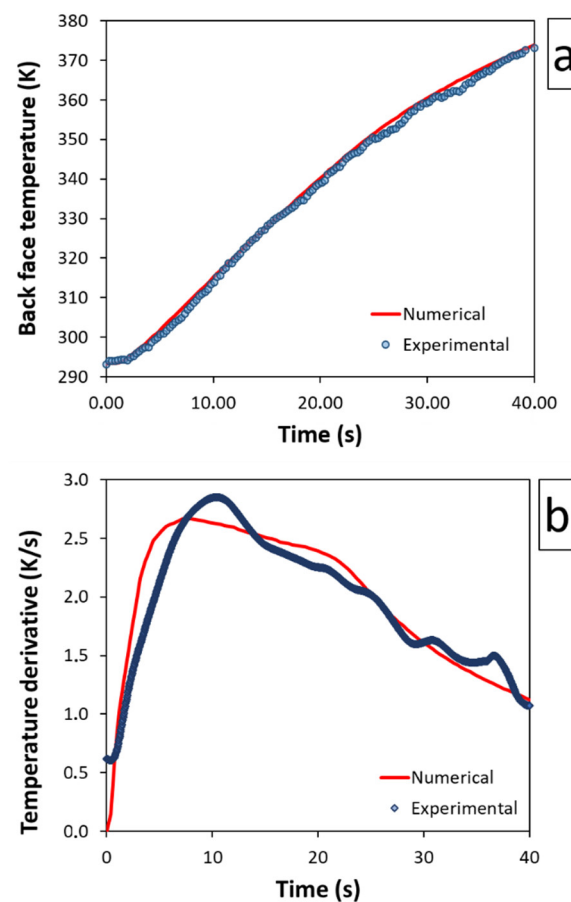


Figure 8. Time evolution of experimentally-observed (symbols) and numerically-computed (lines) data: (a) back-face temperature and (b) its time derivative.

In detail, as it can be noticed from Figure 8a, after applying the heat source over the top face at $t = 0$, the temperature starts monotonically increasing. As long as the temperature is below the activation threshold T_s , the coating is still at its initial thickness, whereas the back-face temperature follows closely the temperature in top face, according to classical Fourier law. Once the temperature reaches the activation threshold at $t = 20.8$ s, the swelling process begins and the back-face temperature grows more slowly. Indeed, the growth rate of the back-face temperature exhibits a significant reduction, as depicted in Figure 8b, so contributing to the thermal insulation of the steel layer from the heat source. This is confirmed by the temperature trend over time for the entire investigated process, shown in Figure 6, in which, upon reaching the threshold time, an evident variation in the slope of the curves relating to the coated samples (iC and APiC) is noted. The slopes of the temperature trend over the time of the uncoated sample (uC) are much steeper.

A similar agreement between experimental and simulated data holds for the evolution of the overall thickness of ablative and growing layers, as shown in Figure 9. Indeed, for $T < T_s$ (namely for $t < 20.8$ s), the overall thickness is kept fixed at $g(t) - x_{steel} = x_{abla} = 0.76$ mm, whereas, for $T > T_s$, the overall thickness increases substantially by even one order of magnitude, reaching the value of about 7 mm, as confirmed by the data reported in Table 2, in which the thickness of the APiC sample at 40 s, when the activation of the intumescence process has been reached, is 6.6 mm.

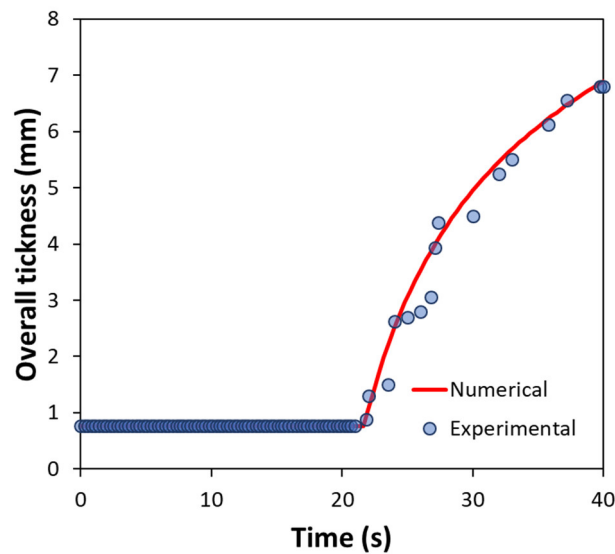


Figure 9. Comparison between the time evolution of experimental (symbols) and numerical (lines) overall thickness of ablative and growing layers.

Moreover, since the decomposition of the ablative layer is not accessible experimentally, its time evolution is monitored through numerical simulations. The results depicted in Figure 10 reveal that, after about 40 s, the consumption of the coating layer is almost complete, as the remaining thickness amounts to about 0.13 mm.

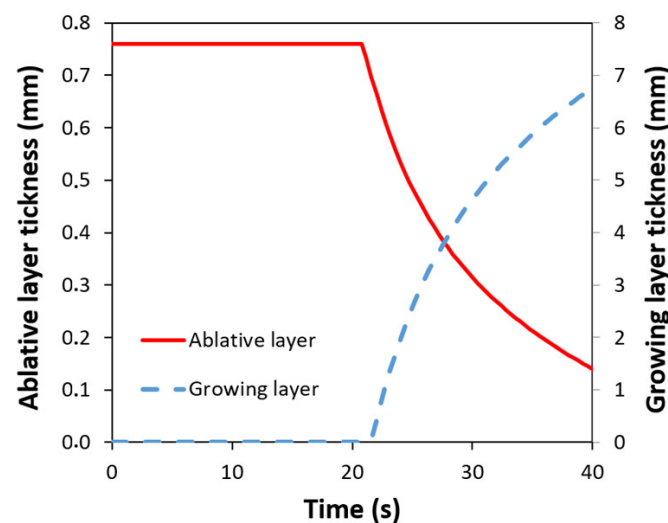


Figure 10. Numerical prediction of the time evolution of the ablative layer thickness.

In fact, as shown in Table 2, observing the thickness of the the APiC sample at different time, at 25 and 40 s, an increase of 113% can be noted. The effect of the swelling is significantly reduced from 40 to 65 s (60%), just before subtracting the flame from the surface of the specimen. This is due to the reduction of the ablative layer. Its consumption, as predicted in Figure 10, influences the production of the growing layer, decreasing the growing rate.

4. Conclusions

In this paper, the intumescent capacity of two different composite coatings, in which the active components are ammonium polyphosphate and pentaerythritol was investigated. The sample was exposed to a gas-torch flame for 70 s, and the temperature on the back of the sample was recorded throughout the test, by means of a K-thermocouple. The

results highlight that iC and APiC coatings exhibit a clear intumescent and barrier capacity. The two formulations exhibit a different amount of ammonium polyphosphate filler, in particular, the APiC sample, which presents the higher percentage, exhibits 29 wt.% of ammonium polyphosphate. Best results were observed for APiC batch where the porous char, formed during exposure to direct flame, appears more regular and thicker than iC one. Furthermore, the acquired thermal profiles evidence that APiC samples show a maximum temperature of about 23 K lower than iC, confirming the higher thermal barrier capacity supplied by this coating formulation. The experimental data were further investigated by comparing the two intumescent formulations with an uncoated steel plate. The insulating behavior of the coatings was confirmed and a decrease in temperature of about 200 K was recorded. Moreover, the higher presence of ammonium polyphosphate favors the formation of a thicker (12.2 mm after 65 s of flame exposure) and more distributed intumescent product on the steel plate, which leads to a better insulating effect of the coating (457.4 K vs. 480.4 K, for APiC and iC, respectively).

Furthermore, a theoretical model was used to describe the insulating properties of an intumescent coating, deposited on a steel plate. The theoretical results were compared to the experimental ones, carried out by means of a flame test and using a heat flux of 150 kW/m² to better discriminate the phenomena that occur during the intumescence growth process. The experimental data fit well with the theoretical ones, so validating the mathematical model. Through the study of the swelling evolution, it was also possible to define a predictive model for the growth process of the intumescent product, as well as on the rate of the carbonaceous product formation. As the ablative layer is consumed by the intumescence process, the rate, at which the growing layer is formed, decreases.

Author Contributions: Conceptualization, E.P. (Elpida Piperopoulos); methodology, G.S.; software, G.C. and G.G.; validation, E.P. (Elpida Piperopoulos), G.S., G.G. and G.C.; formal analysis, G.C. and G.G.; investigation, G.S., E.P. (Elpida Piperopoulos), G.C. and G.G.; resources, E.P. (Edoardo Proverbio); data curation, G.S., E.P. (Elpida Piperopoulos) and L.C.; writing—original draft preparation, E.P. (Elpida Piperopoulos) and G.C.; writing—review and editing, L.C. and M.A.; visualization, G.S. and L.C.; supervision, E.P. (Edoardo Proverbio) and M.A.; funding acquisition, E.P. (Edoardo Proverbio) and M.A. All authors have read and agreed to the published version of the manuscript.

Funding: This research was funded by PO FESR SICILIA 2014–2020, Project 08TP20120000244 NO FIRE NAVE—Nuova formulazione di rivestimenti antifiamma per il settore navale, CUP G38I18000970007.

Institutional Review Board Statement: Not applicable.

Informed Consent Statement: Not applicable.

Data Availability Statement: Data is contained within this article.

Acknowledgments: The authors thank Antonino Valenza of the Engineering Department of the University of Palermo, scientific manager of the NO FIRE NAVE project.

Conflicts of Interest: The authors declare no conflict of interest.

References

1. Eleven Passengers Missing in Greece Ferry Fire—CNN. Available online: <https://edition.cnn.com/2022/02/18/europe/greek-ferry-fire-scli-intl/index.html> (accessed on 11 July 2022).
2. Vairo, T.; Quagliati, M.; Del Giudice, T.; Barbucci, A.; Fabiano, B. From land- to water-use-planning: A consequence based case-study related to cruise ship risk. *Saf. Sci.* **2017**, *97*, 120–133. [[CrossRef](#)]
3. Gravit, M.; Dmitriev, I. Numerical simulation of fire resistance of steel ship bulkheads. *Transp. Res. Procedia* **2021**, *54*, 733–743. [[CrossRef](#)]
4. Piperopoulos, E.; Scionti, G.; Atria, M.; Calabrese, L.; Proverbio, E. Flame-retardant performance evaluation of functional coatings filled with Mg(OH)₂ and Al(OH)₃. *Polymers* **2022**, *14*, 372. [[CrossRef](#)]
5. Mariappan, T. Recent developments of intumescent fire protection coatings for structural steel: A review. *J. Fire Sci.* **2016**, *34*, 120–163. [[CrossRef](#)]
6. Elliott, A.; Temple, A.; Maluk, C.; Bisby, L. Novel testing to study the performance of intumescent coatings under non-standard heating regimes. *Fire Saf. Sci.* **2014**, *11*, 652–665. [[CrossRef](#)]
7. Camino, G.; Costa, L.; Martinasso, G. Intumescent fire-retardant systems. *Polym. Degrad. Stab.* **1989**, *23*, 359–376. [[CrossRef](#)]

8. Wladyka-Przybylak, M.; Kozlowski, R. The thermal characteristics of different intumescent coatings. *Fire Mater.* **1999**, *23*, 33–43. [[CrossRef](#)]
9. Lucherini, A.; Maluk, C. Assessing the onset of swelling for thin intumescent coatings under a range of heating conditions. *Fire Saf. J.* **2019**, *106*, 1–12. [[CrossRef](#)]
10. Li, G.-Q.; Zhang, C.; Lou, G.-B.; Wang, Y.-C.; Wang, L.-L. Assess the fire resistance of intumescent coatings by equivalent constant thermal resistance. *Fire Technol.* **2012**, *48*, 529–546. [[CrossRef](#)]
11. Wang, L.; Dong, Y.; Zhang, C.; Zhang, D. Experimental study of heat transfer in intumescent coatings exposed to non-standard furnace curves. *Fire Technol.* **2015**, *51*, 627–643. [[CrossRef](#)]
12. Taylor, A.P.; Sale, F.R. Thermoanalytical studies of intumescent systems. *Makromol. Chemie. Macromol. Symp.* **1993**, *74*, 85–93. [[CrossRef](#)]
13. Di Blasi, C.; Branca, C. Mathematical model for the nonsteady decomposition of intumescent coatings. *AIChE J.* **2001**, *47*, 2359–2370. [[CrossRef](#)]
14. Cirpici, B.K.; Wang, Y.C.; Rogers, B.D.; Bourbigot, S. A theoretical model for quantifying expansion of intumescent coating under different heating conditions. *Polym. Eng. Sci.* **2016**, *56*, 798–809. [[CrossRef](#)]
15. Anderson, C.E.; Wauters, D.K. A thermodynamic heat transfer model for intumescent systems. *Int. J. Eng. Sci.* **1984**, *22*, 881–889. [[CrossRef](#)]
16. Di Blasi, C. Modeling the effects of high radiative heat fluxes on intumescent material decomposition. *J. Anal. Appl. Pyrolysis* **2004**, *71*, 721–737. [[CrossRef](#)]
17. Gillet, M.; Autrique, L.; Perez, L. Mathematical model for intumescent coatings growth: Application to fire retardant systems evaluation. *J. Phys. D Appl. Phys.* **2007**, *40*, 883–899. [[CrossRef](#)]
18. Griffin, G.J. The modeling of heat transfer across intumescent polymer coatings. *J. Fire Sci.* **2009**, *28*, 249–277. [[CrossRef](#)]
19. Zhang, Y.; Wang, Y.C.; Bailey, C.G.; Taylor, A.P. Global modelling of fire protection performance of intumescent coating under different cone calorimeter heating conditions. *Fire Saf. J.* **2012**, *50*, 51–62. [[CrossRef](#)]
20. Delobel, R.; Bras, M.L.; Ouassou, N.; Alistiqsa, F. Thermal behaviours of ammonium polyphosphate-pentaerythritol and ammonium pyrophosphate-pentaerythritol intumescent additives in polypropylene formulations. *J. Fire Sci.* **1990**, *8*, 85–108. [[CrossRef](#)]
21. Lucherini, A.; Maluk, C. Intumescent coatings used for the fire-safe design of steel structures: A review. *J. Constr. Steel Res.* **2019**, *162*, 105712. [[CrossRef](#)]
22. Staggs, J.E.J. A simple model of polymer pyrolysis including transport of volatiles. *Fire Saf. J.* **2000**, *34*, 69–80. [[CrossRef](#)]
23. Mousquès, P.; Dirion, J.L.; Grouset, D. Modeling of solid particles pyrolysis. *J. Anal. Appl. Pyrolysis* **2001**, *58–59*, 733–745. [[CrossRef](#)]
24. Chaisaenrith, P.; Taksakulvith, P.; Pavasupree, S. Effect of nano titanium dioxide in intumescent fireproof coating on thermal performance and char morphology. *Mater. Today Proc.* **2021**, *47*, 3462–3467. [[CrossRef](#)]
25. Anderson, C.E.; Ketchum, D.E.; Mountain, W.P. Thermal conductivity of intumescent chars. *J. Fire Sci.* **1988**, *6*, 390–410. [[CrossRef](#)]
26. Zybina, O.; Gravit, M.; Stein, Y. Influence of carbon additives on operational properties of the intumescent coatings for the fire protection of building constructions. *IOP Conf. Ser. Earth Environ. Sci.* **2017**, *90*, 12227–12230. [[CrossRef](#)]
27. Banerjee, D.K. An analytical approach for estimating uncertainty in measured temperatures of concrete slab during fire. *Fire Saf. J.* **2016**, *82*, 30–36. [[CrossRef](#)]
28. Kramer, M.A.; Greiner, M.; Koski, J.A.; Lopez, C. Uncertainty of heat transfer measurements in an engulfing pool fire. In *Astm Special Technical Publication*; ASTM: West Conshohocken, PS, USA, 2003; pp. 111–127.
29. Banerjee, D.K. Uncertainties in steel temperatures during fire. *Fire Saf. J.* **2013**, *61*, 65–71. [[CrossRef](#)]